Assignment of the G^+ and G^- Raman bands of metallic and semiconducting carbon nanotubes based on a common valence force field

Eugenio Di Donato, Matteo Tommasini, Chiara Castiglioni, and Giuseppe Zerbi
Dipartimento di Chimica, Materiali ed Ingegneria Chimica "G. Natta," Politecnico di Milano, Piazza Leonardo da Vinci 32, Milano, Italy
and INSTM, UdR Milano, Italy

(Received 5 December 2005; revised manuscript received 26 July 2006; published 9 November 2006)

We propose a model for calculating the phonon frequencies of any (n,m) nanotube by considering explicitly the curvature of the system and the effects of long-range interactions determined by π electrons. We show that the electron-phonon coupling strength is directly related to the electronic structure of the nanotube and it is the main interaction responsible for the different behavior shown in the Raman spectra by metallic and semiconducting nanotubes. On the basis of the vibrational valence force field derived in this work we propose an assignment of the G band. Moreover, based on symmetry-selection rules, we can state that the LO modes of armchair nanotubes and the TO modes of zigzag nanotubes at $\mathbf{\Gamma}_0$ are silent in the Raman spectra.

DOI: 10.1103/PhysRevB.74.184306 PACS number(s): 63.20.Dj, 73.63.Fg, 78.30.−j, 73.22.−f

I. INTRODUCTION

The interpretation of the Raman spectra of single-walled carbon nanotubes (SWNT's) presents still open questions. In particular, the G band of SWNT samples exhibits a structured shape which depends on the peculiar electronic structure of the nanotube and is due to the symmetry-breaking effects produced by the wrapping of the graphene sheet around a cylindrical surface. It is known that the higher frequency G^+ peak is practically independent of the nanotube diameter ($\omega_G^+=1591\ \mathrm{cm}^{-1}$), while the dispersion of the lower-frequency G^- peak can be described according to the empirical fit $\omega_G^-=\omega_G^+-C/d_t^2$, with C being a different coefficient for metallic and semiconducting nanotubes ($C_m>C_s$).[1]

In this work we propose a general model for computing the phonon frequencies of any (n,m) nanotube based on a suitably developed force field. The outcomes of the model lead us to a unified interpretation of G-band behavior in the Raman spectra of metallic and semiconducting SWNT's. Moreover, our model is able to predict the right linear dispersion of the radial breathing mode (RBM) with respect to the inverse diameter of the nanotube.

Our approach does not rely on first-principles calculations or zone folding of graphite, but merely extends the use of empirical valence force field calculations from the domain of polyconjugated polymers[2,3] and graphite[4] to the domain of nanotubes. This choice is based on our previous experience in developing a semiempirical force field for graphite and related molecular compounds.[4] On the other hand, it is well known that for systems characterized by a network of covalent bonds, a valence force field is built upon parameters which are much closer to "chemical intuition" than any Cartesian force constants. For this reason these parameters are straightforwardly transferable when one considers systems characterized by a similar chemical structure. On the basis of valence coordinates[5] the dynamical problem is written as

$$(\mathbf{GF})\mathbf{L}=\omega^2\mathbf{L}, \tag{1}$$

where $\mathbf{G}$ and $\mathbf{F}$ are, respectively, the kinetic and dynamical matrices which are defined following Wilson *et al.*;[5] ω is the vibrational frequency of a given mode, and $\mathbf{L}$ is the corresponding eigenvector in terms of displacements along internal coordinates. We describe the internal coordinates of any nanotube through the internal coordinates of the graphene cell wrapped around the cylinder of radius $R=|\mathbf{C}_h|/2\pi$ (details are found in Appendix A). These are a total of nine internal degrees of freedom (three stretchings and six bendings; see Fig. 1). The real curved structure of the whole nanotube can be generated by applying a suitable rototraslation to this unit cell (see Appendix A). In this way we can take into account the effect of the real geometrical structure of the nanotube on the phonon frequencies. The dynamical problem is treated in terms of phonon coordinates built on the basis of the few degrees of freedom of the minimal structural unit. The advantage of this treatment lies, on the one hand, in the fact that the phonon frequencies can be obtained through the diagonalization of a small dynamical matrix (i.e., a 9×9 matrix). On the other hand, and even more important, we obtain a formally identical problem for any nanotube we would like to consider. While the effect of a different curvature is described by the kinetic matrix $\mathbf{G}$, the differences among the dynamical couplings associated with different electronic structures (namely, differences between metallic and semiconducting nanotubes[6]) *must* be described through a different $\mathbf{F}$ matrix. In particular, due to the Kohn

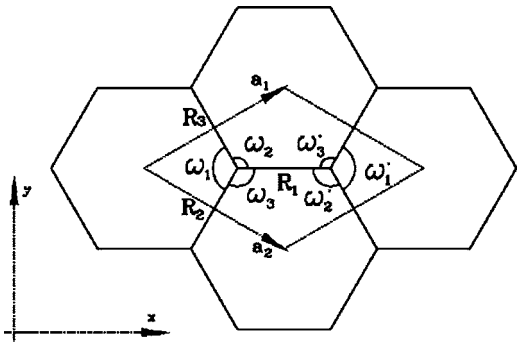

FIG. 1. Definition of the valence coordinates for a generic (n,m) nanotube.

anomaly,[6,7] we need a model which can distinguish a system with long-range interactions (metallic) from a system with shorter-range interactions (semiconducting). A simple model which is known to treat accurately CC stretching interactions in polyconjugated systems is based on Hückel theory.[2,3] Within the same frame, following the derivation introduced by Coulson and Longuet-Higgins,[8–10] Kakitani developed expressions for the valence force constants involving CC stretchings.[11] The force field used in this work for nanotubes is the one adapted to small Polycyclic Aromatic Hydrocarons (PAH's) by Ohno[12] following Kakitani's work. We have recently shown that this force field is able to describe systems with strong electron-phonon coupling (EPC).[13] The Ohno force field has been developed for planar molecules[12] and therefore extended to the graphene sheet.[4] For these cases the vibrational problem can be exactly factorized into two independent problems: namely, the in-plane and the out-of-plane one. Thanks to this property Ohno's force field does not contain the definition of the out-of-plane degrees of freedom and related force constants. This procedure does not affect at all the calculation of frequencies associated with in-plane modes, which can be indeed exactly described through this approach. In the case of carbon nanotubes a straightforward generalization of Ohno's force field cannot be done since separation (by symmetry) between in-plane and out-of-plane modes is no longer possible. In spite of this we restrict ourselves to those coordinates (bendings and stretchings) which represent a complete set of vibrational coordinates for the in-plane vibrational problem in the limiting case of a nanotube with infinite diameter (i.e., graphene). In other words, in the present treatment we restrict ourselves to the force constants defined in the original Ohno work; i.e., we do not include any internal coordinate defining torsions around carbon-carbon bonds. Nevertheless, thanks to ring redundancies between valence coordinates in systems containing aromatic rings,[14] the valence coordinates adopted in this work form a complete basis set for the description of the whole vibrational space of SWNT's. On the other hand, the lack of a definition of specific force constants for the torsional degrees of freedom is expected to cause poor results for the low-frequency phonon branches. It is, however, important to note that in the case of the radial breathing mode (RBM) at $\mathbf{\Gamma}_0$, which is the vibration responsible for the main Raman band observed at low frequencies, the vibrational displacements do not imply any angular (nor torsional) change, since the nanotube merely expands or shrinks while keeping exactly the same shape. For this reason the prediction of RBM frequencies is not affected by the lack of torsional force constants in our model. Moreover, the high-frequency G modes, which are the center of the present discussion, are certainly unaffected by couplings with torsional vibrations, because of the large difference between their characteristic energies.

II. DISCUSSION OF THE MODEL

The $\mathbf{G}$ matrix in Eq. (1) allows us to describe the kinetic energy T in internal coordinates, $2T=\dot{\mathbf{R}}^{\dagger}\mathbf{G}^{-1}\dot{\mathbf{R}}$. It is expressed as follows:[5]

$$\mathbf{G} = \mathbf{B}\mathbf{M}^{-1}\mathbf{B}^{\dagger}, \tag{2}$$

where $\mathbf{M}$ is the diagonal matrix of the atomic masses and $\mathbf{B}$ is the transformation which relates the Cartesian coordinates to the internal coordinates ($\mathbf{R}=\mathbf{B}\mathbf{X}$). For periodic systems the $\mathbf{B}$ matrix can we written in the following way:[4,15]

$$\mathbf{B}(\theta_1,\theta_2) = \mathbf{B}_{00} + \mathbf{W}(-\phi_1)\mathbf{B}_{10}\mathbf{e}^{i\theta_1} + \mathbf{W}(\phi_1)\mathbf{B}_{\bar{1}0}\mathbf{e}^{-i\theta_1} + \mathbf{W}(-\phi_2)\mathbf{B}_{01}\mathbf{e}^{i\theta_2} + \mathbf{W}(\phi_2)\mathbf{B}_{0\bar{1}}\mathbf{e}^{-i\theta_2}. \tag{3}$$

The auxiliary matrices $\mathbf{B}_{10}$, $\mathbf{B}_{01}$, etc., are defined in Appendix A; $\theta_i=\mathbf{a}_i\cdot\mathbf{k}$—i.e., $\mathbf{k}=(\theta_1\mathbf{b}_1+\theta_2\mathbf{b}_2)/(2\pi)$—and $\mathbf{W}(\phi)$ is a suitable rotation matrix [see Eq. (A6) and Appendix A]. According to Eq. (3), $\mathbf{B}(\theta_1,\theta_2)$ defines the Bloch internal coordinates on the basis of the Cartesian atomic displacements—i.e., $\mathbf{R}(\theta_1,\theta_2)=\mathbf{B}(\theta_1,\theta_2)\mathbf{X}^{(0,0)}$. For the details see Appendix A. Note that the variables θ_1 and θ_2 simply represent the phase differences of vibrational displacements between nearest-neighboring cells along the $\mathbf{a}_1$ or $\mathbf{a}_2$ direction. It is important to realize that the Wilson's vectors entering the $\mathbf{B}$ matrix are constructed by using the true curved geometry of the nanotube (see Appendix A). This makes it possible to account for curvature effects in dealing with the basic dynamical problem given by Eq. (1).

Since the allowed wave vectors in SWNT's do satisfy particular boundary conditions which are the direct consequence of the symmetry of the system, we obtain the following prescriptions for the phase differences (see Appendix B and Ref. 16):

$$\theta_1 = \phi_1\mu + \tau_1\xi,$$

$$\theta_2 = \phi_2\mu + \tau_2\xi, \tag{4}$$

where $\mu\in[0\ldots,(N(n,m)-1)]$ is an integer[17] and ξ assumes values between $-\pi$ and π. The coefficients $\phi_{1,2}$ and $\tau_{1,2}$ are known functions of the (n,m) indices of the nanotube considered (see Appendix A). The closed expressions (4) for θ_1 and θ_2 account for the periodic boundary conditions of any (n,m) nanotube. In the literature[18] the same conditions are usually expressed in terms of the $\mathbf{k}$ wave vector, the chiral vector $\mathbf{C}_h$, and the translation vector $\mathbf{T}$ (see Appendix B):

$$\mathbf{k}\cdot\mathbf{C}_h = 2\pi\mu,$$

$$\mathbf{k}\cdot\mathbf{T} = \xi. \tag{5}$$

The particular choice $\xi=0$, $\mu\in[0\ldots,N-1]$, corresponds to selecting phonons which do satisfy the condition $\mathbf{q}=\mathbf{0}$ within the first Brillouin zone of the given nanotube. In this work we indicate with $\mathbf{\Gamma}_\mu$ ($\mu=0,1,\ldots$) the collection of (θ_1,θ_2) values at $\xi=0$ given by Eq. (4). These points correspond to the potentially Raman active phonons.[19]

A. Force field

The elements of the force constant matrix $\mathbf{F}$ for a periodic system can be written employing the Bloch theorem as follows (i and j label a given internal coordinate, and n_1 and n_2 denote the cell position in the lattice):[15]

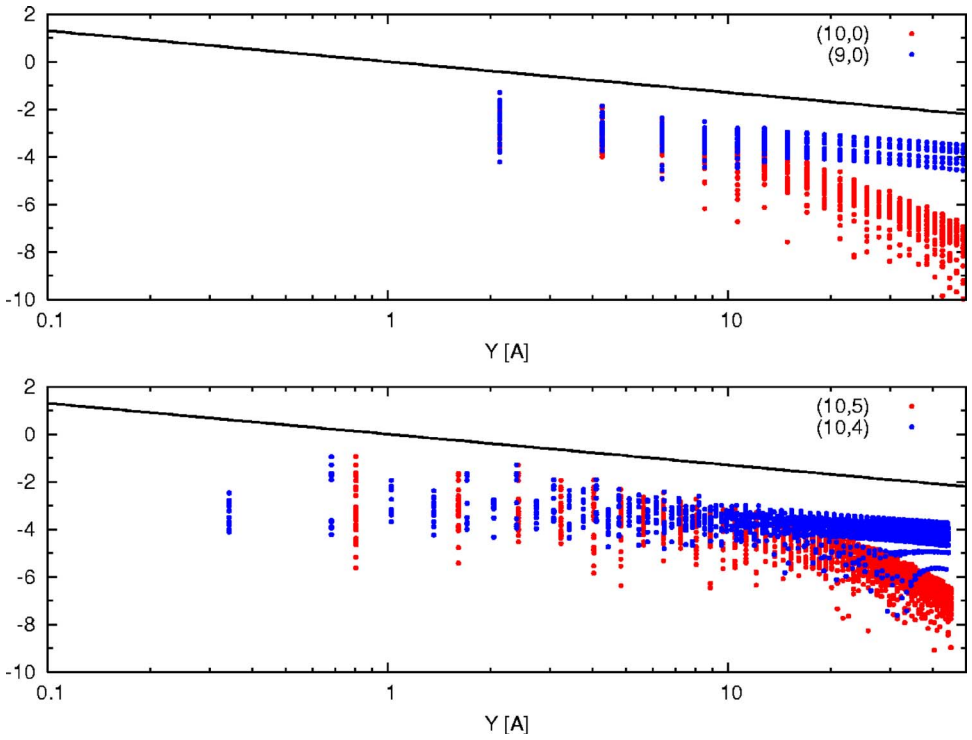

FIG. 2. (Color online) Decrease of the absolute value of the BBP (logarithmic scale, $\log_{10}|\Pi_{ij}|$) as a function of the distance Y between the (0,0) reference cell and the (n_1,n_2) cell where the jth bond lies. The distance is projected along the nanotube axis. Blue points are for metallic nanotubes and red points for semiconducting nanotubes. The function $f=Y^{-1.3}$ is also shown in the plot as a guide to the eye.

$$F_{ij}(\theta_1,\theta_2)=\sum_{n_1,n_2} f_{i_{0,0}j_{n_1,n_2}} e^{i(n_1\theta_1+n_2\theta_2)}. \tag{6}$$

Following Kakitani,[11] the force constant f_{ij} relative to the interaction between ith and jth CC stretching coordinates is given by

$$f_{ij}=\left(k_\sigma+2\frac{\partial^2\beta}{\partial R^2}p_i\right)\delta_{ij}+2\left(\frac{\partial\beta}{\partial R}\right)^2\Pi_{ij},$$

$$i\equiv i_{0,0},\quad j\equiv j_{n_1,n_2}, \tag{7}$$

where β is the resonance integral in the frame of Hückel theory, p_i represents the bond order of the ith carbon-carbon bond, and Π_{ij} is the bond-bond polarizability (BBP). This latter quantity expresses the change in the ith bond order induced by a change in the hopping integral of the jth bond or, equivalently, the second-order change of energy induced by the change in the hopping integral relative to bonds ith and jth.[8] Ohno's force field makes use of Eq. (7), taking the benzene molecule as reference system. By denoting with p_0 and Π_0 the bond order and self-polarizability of the CC bonds of benzene, Eq. (7) becomes

$$f_{ii}=f_1+f_2(p_i-p_0)+f_3(\Pi_{ii}-\Pi_0),$$

$$f_{ij}=f_3\Pi_{ij},\quad i\neq j. \tag{8}$$

Explicit expressions for the constants f_1, f_2, and f_3 can now be obtained by substituting $p_i=p_0$, $\Pi_{ii}=\Pi_0$ into Eq. (7). This results in the following set of parameters:[12]

$$f_1=k_\sigma+2\frac{\partial^2\beta}{\partial R^2}p_0+2\left(\frac{\partial\beta}{\partial R}\right)^2\Pi_0$$

$$=k_\sigma+f_2p_0+f_3\Pi_0=6.821\ \text{N/cm},$$

$$f_2=2\frac{\partial^2\beta}{\partial R^2},\quad f_2=5.450\ \text{N/cm},$$

$$f_3=2\left(\frac{\partial\beta}{\partial R}\right)^2,\quad f_3=3.646\beta_0\text{N/cm}. \tag{9}$$

Ohno's force field introduces eight semiempirical parameters $(f_1,f_2,\ldots,f_8)$ which have been determined by a fitting procedure based on the experimental vibrational frequencies of small polycyclic aromatic hydrocarbons.[12] For defining the subspace of the CC stretching coordinates just the three parameters (f_1,f_2,f_3) appearing in Eq. (9) are required. The quantities p_i and Π_{ij} can be determined for each nanotube, once and for all, after diagonalizing the Hückel Hamiltonian of the specific (n,m) nanotube considered (see Appendix C). The quantities p_i and Π_{ij} contain all the needed information on the π electronic structure and on the topology of the system considered. The effect of the Kohn anomaly recently pointed out in graphite and carbon nanotubes[6,7] is fully included in the polynomial decay of the force constants in real space, ruled by the behavior of the BBP Π_{ij} [see Fig. 2 and Eq. (7)]. From the analysis of Fig. 2 it is clear that the dynamical interactions in metallic nanotubes have a longer range than in semiconducting nanotubes. According to Eq. (9) one realizes that the f_3 parameter is directly related to the electron phonon-coupling parameter $\partial\beta/\partial R$ as it is defined in the Hückel frame.[13] In particular, f_3 is precisely the coefficient which turns the BBP into an off-diagonal CC stretching force constant [see Eq. (8)]. As for the other five Ohno parameters they describe diagonal force constants of bending coordinates and bending-stretching interactions which are taken as short-range empirical terms. Among these five parameters, only two constants are needed for the present nano-

tube force field: (i) $f_5=0.928\times10^{-8}$ N/rad which is the diagonal CCC bending constant and (ii) $f_7=0.430\times10^{-18}$ N m/rad which represents the interaction between nearest-neighbor CC stretching and CCC bending.

As in the case of graphite[4] we decide here to keep all the empirical parameters fixed to the values proposed by Ohno. This will result in an estimate of the vibrational frequencies systematically lower by roughly 35 cm^{-1}. With some effort one could improve the choice of the parameters in order to fit the experimental data on nanotubes. However, the agreement (in terms of trends) that we obtain by using a force field containing empirical parameters which were optimized for rather different systems such as polycyclic aromatic hydrocarbons is already surprisingly good. As already pointed out, the physics of phonons in nanotubes is mainly due to the bond orders p_i and BBP Π_{ij} and not to the particular choice of the f_1, f_2, and f_3 numerical parameters. As a consequence, this force field will naturally distinguish metallic from semiconducting nanotubes since the bond orders and BBP's are extremely sensitive to the electronic structure of the nanotubes considered. This model will therefore provide valuable information on the vibrational structure of nanotubes, with particular emphasis on the *G* band and its dependence on the electronic structure and diameter.

The general expressions for the the bond order p_i and the BBP Π_{ij} in terms of linear combination of atomic orbitals (LCAO) coefficients C and orbital energies ε were determined in the past by[8]

$$p_{\lambda\rho}=\sum_{o}(C_{\lambda o}C_{\rho o}^{*}+C_{\lambda o}^{*}C_{\rho o}),$$

$$\Pi_{\lambda\rho,\nu\sigma}=\sum_{o,e}\frac{(C_{\lambda o}^{*}C_{\rho e}+C_{\lambda e}C_{\rho o}^{*})(C_{\nu o}C_{\sigma e}^{*}+C_{\nu e}^{*}C_{\sigma o})}{\varepsilon_o-\varepsilon_e}+\text{c.c.} \tag{10}$$

In Eq. (10) the labels $\lambda\rho$ and $\nu\sigma$ indicate the pairs of $2p_z$ carbon atomic orbitals involved in two bonds i,j and the sum runs over occupied (o) and empty (e) molecular orbitals. The bond orders and BBP for SWNT's (Ref. 20) are expressed as integrals over the Brillouin zone of the nanotube, similarly to previous studies of systems with periodic boundary conditions:[2–4]

$$p_i=\frac{1}{2\pi N}\sum_{\mu}\int_{-\pi}^{\pi}q_i d\xi,$$

$$\Pi_{i_{(0,0)}j_{(n_1,n_2)}}=\frac{1}{(2\pi N)^2}\sum_{\mu,\mu'}\int_{-\pi}^{\pi}d\xi\int_{-\pi}^{\pi}d\xi'\,\pi_{i_{(0,0)}j_{(n_1,n_2)}}. \tag{11}$$

The integrand functions q_i are defined in Appendix C. The functions π_{ij} are known functions of μ, μ' and ξ, ξ', through $\theta_{1,2}$ and $\theta'_{1,2}$ [see Eq. (4) and Appendix C]. The indexes μ and μ' determine pairs of discrete lines in the reciprocal lattice of graphite, the path of integration being parametrically described by the variables ξ and ξ'. The integration path in the θ_1-θ_2 plane is given by Eq. (4), and it can be seen as a set of segments in the θ_1-θ_2 plane whose slope and lengths are functions of the coefficients $\phi_{1,2}$ and $\tau_{1,2}$ which are in turn functions of (n,m) according to Eq. (A5). It is clear that the functions π_{ij} are formally equal for any nanotube but the path of integration is different for each nanotube. In particular, for metallic nanotubes the path of integration will include the **K** (**K**′) points. We therefore have introduced a treatment of vibrations which knows both the real three-dimensional geometry of the nanotube through the kinetic energy matrix **G** and the peculiar electronic structure through p_i and Π_{ij} and, by consequence, through the force field **F**.

TABLE I. List of the nanotubes studied in this work.

Armchair	Zigzag	Chiral		
(6,6)	(9,0)	(6,3)	(6,2)	(5,2)
(7,7)	(10,0)	(8,4)	(9,3)	(10,4)
(10,10)	(15,0)	(10,5)	(12,4)	(15,6)
(11,11)	(16,0)	(12,6)		
(12,12)	(18,0)	(14,7)		
(14,14)	(20,0)			
(17,17)	(23,0)			
(21,21)	(24,0)			

III. RESULTS

In this section we show the results obtained by using our valence force field on different nanotubes. The nanotubes investigated are listed in Table I. For all the nanotubes we have computed the phonon dispersion curves. Typical results are shown in Figs. 3 and 4. As already discussed in Sec. I the phonon dispersion curves here presented are not accurate for the low-frequency modes since the present force field does not contain interactions associated with torsional degrees of freedom. The phonon dispersions are given here to merely show the efficacy of the method and its straightforward applicability to any nanotube. Moreover, by directly inspecting the phonon dispersions in the *G*-band region (which is accurately described in the present treatment) the behavior of the Kohn anomaly can be more easily assessed.

We observe that all the phonon dispersions of the metallic nanotubes reported in Figs. 3 and 4 show a marked Kohn anomaly at $\mathbf{\Gamma}_0$ as expected according to the literature.[6] We observe also that the (9, 0) and (6, 3) nanotubes [Figs. 3(b) and 4(b)] exhibit the Kohn anomaly not only at $\mathbf{\Gamma}_0$ but also at some $\mathbf{\Gamma}_\mu$ with $\mu\neq0$. For instance for the (9, 0) nanotube we observe the Kohn anomaly at $\mathbf{\Gamma}_6$ and $\mathbf{\Gamma}_{12}$ and for the (6, 3) nanotube we observe the Kohn anomaly at $\mathbf{\Gamma}_{14}$ and $\mathbf{\Gamma}_{28}$. This happens for all the (metallic) nanotubes for which the **K** point of graphene corresponds to a given $\mathbf{\Gamma}_\mu$ point. Since $\mathbf{\Gamma}_\mu$ is defined by Eqs. (4) with the condition $\xi=0$, the requirements $\mathbf{\Gamma}_\mu=\mathbf{K}$, $\mathbf{\Gamma}_\mu=\mathbf{K}'$ reduce to the following conditions:

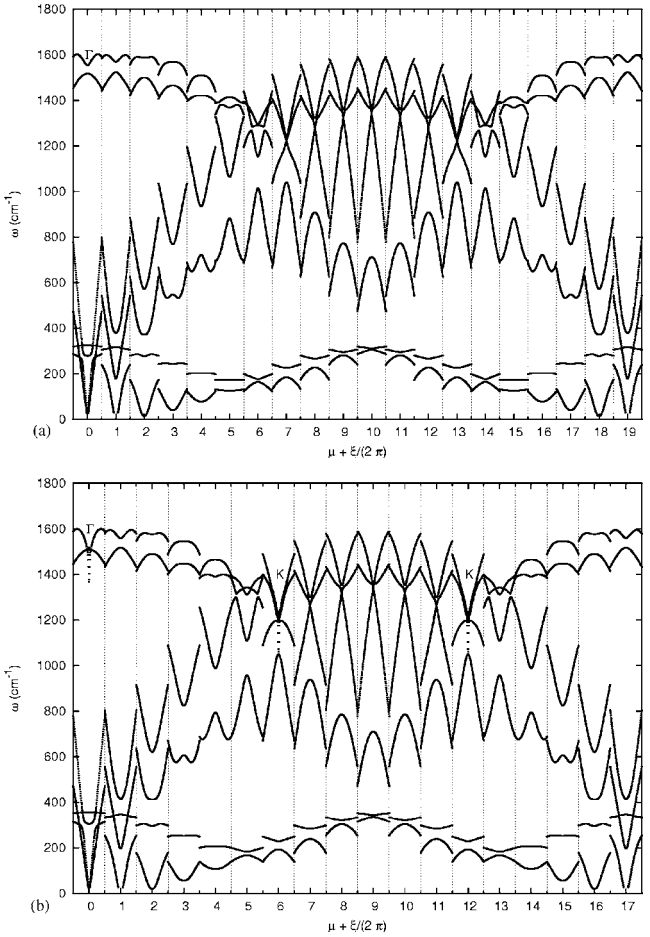

FIG. 3. Phonon dispersion curves of one semiconducting and one metallic nanotube computed with the valence force field proposed in the present work. (a) (10, 0) semiconducting zigzag and (b) (9, 0) metallic zigzag.

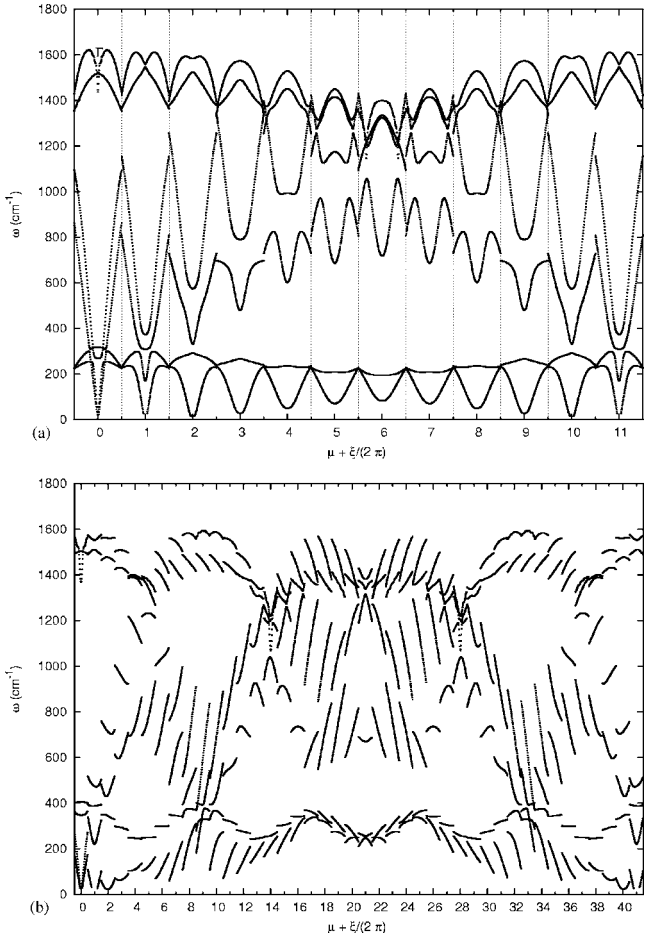

FIG. 4. Phonon dispersion curves of two metallic nanotubes computed with the valence force field proposed in the present work. (a) (6, 6) armchair and (b) (6, 3) metallic chiral.

$$\mu\phi_1 = +\frac{2}{3}\pi + 2\pi p_1,$$

$$\mu\phi_2 = -\frac{2}{3}\pi + 2\pi p_2,$$

$$\mu\phi_1 = -\frac{2}{3}\pi + 2\pi h_1,$$

$$\mu\phi_2 = +\frac{2}{3}\pi + 2\pi h_2, \qquad (12)$$

where $(2\pi/3+2\pi p_1, -2\pi/3+2\pi p_2)$ and $(-2\pi/3+2\pi h_1, 2\pi/3+2\pi h_2)$ are the coordinates of **K** and **K′**, respectively (p,h are integer numbers). Recalling that the $\mathbf{q}=\mathbf{0}$ selection rule traduces in selecting only the phonons found at $\mathbf{\Gamma}_\mu$, we can immediately state that only the subset of metallic nanotubes which satisfies the conditions given by Eqs. (12) can potentially exhibit in the Raman spectrum a band associated with the **K**-point phonon (i.e., an intrinsic *D* peak, not necessarily activated by disorder or confinement).

The calculations illustrated in Figs. 3 and 4 have been carried out by using the same parameters proposed by Ohno[12] [see also Eq. (9) and points (i) and (ii) above]. We neglect any f_{ij} force constant relative to the *j*th bond located in a (n_1,n_2) cell at distance larger than $\approx$45 Å (along the nanotube axis) from the (0,0) cell (where the *i*th bond lies). By following this procedure we effectively use a different cutoff for the off-diagonal force constants f_{ij} in metallic with respect to semiconducting nanotubes. This is due to the different decay of the BBP's in the two systems. For instance, at the threshold distance of 45 Å the lowest f_{ij} force costants are of the order of 10^{-6} N/cm for metallic nanotubes while they fall to approximately 10^{-9} N/cm for semiconducting nanotubes (see bottom panel of Fig. 2). This is further evidence that metallic nanotubes exhibit a stronger electron-phonon coupling.[6]

By using our valence force field we have computed the phonon frequencies at $\mathbf{\Gamma}_0$ (i.e., $\xi=0$, $\mu=0$) for the different nanotubes of Table I. By plotting the vibrational frequencies against the diameter, we obtain the trend reported in Fig. 5.

The analysis of the eigenvectors allows us to determine the character of the phonons associated with the calculated frequencies. In particular, we follow here the usual definition of the transversal (longitudinal) character of a phonon as

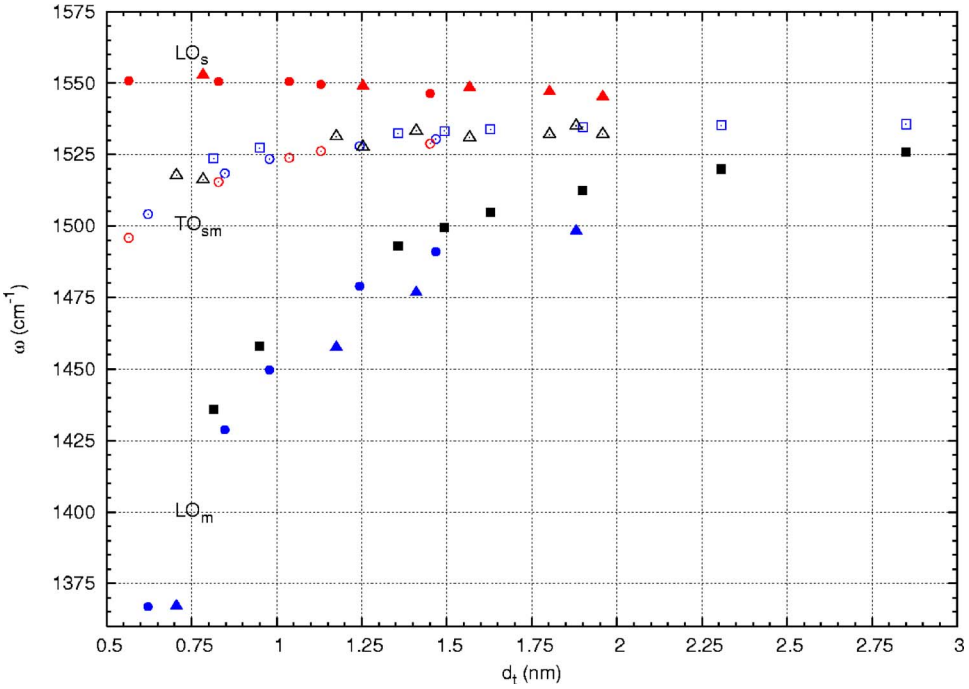

FIG. 5. (Color online) Diameter dependence of the G peaks (at the $\mathbf{\Gamma}_0$ point) in the Raman spectra of nanotubes. Red symbols are associated with semiconducting nanotubes, blue symbols to metallic nanotubes. Solid symbols indicate LO modes; open symbols represent TO modes. Triangles indicate zigzag nanotubes; squares armchair nanotubes and circles are associated with chiral nanotubes. Black symbols indicate silent modes in the Raman spectra of achiral nanotubes.

given by the orthogonal (parallel) direction of the nuclear displacements with respect to the **q** wave vector. Since the **q** wave vector is necessarily parallel to the nanotube axis, it is indeed straightforward to judge whether a mode is transversal or longitudinal by simply inspecting the direction of the nuclear displacements with respect to the nanotube axis. Based on the results of our calculations at $\mathbf{\Gamma}_0$, we therefore assign (a) the G^+ branch to LO (axial) modes of semiconducting nanotubes, (b) the G^- upper branch to TO (transversal) modes of metallic and semiconducting nanotubes, and (c) the G^- lower branch to LO modes of metallic nanotubes.

The simple sketch reported in Fig. 6 shows our interpretation of the G-band dispersion in the Raman spectra of SWNT's. The G^- higher branch (central branch) is due to the dispersion of TO modes of metallic and semiconducting nanotubes. We observe that the TO modes of both metallic and semiconducting nanotubes are sensible to the diameter of the nanotube as expected based on a purely geometric interpretation (see Fig. 5). Moreover, the dispersion with the diameter of the TO modes frequencies is the same for metallic and semiconducting nanotubes. In semiconducting nanotubes the G modes do not suffer a marked electron-phonon coupling. As a consequence, we obtain a LO mode that is practically not diameter dependent (see Fig. 5). Instead, the

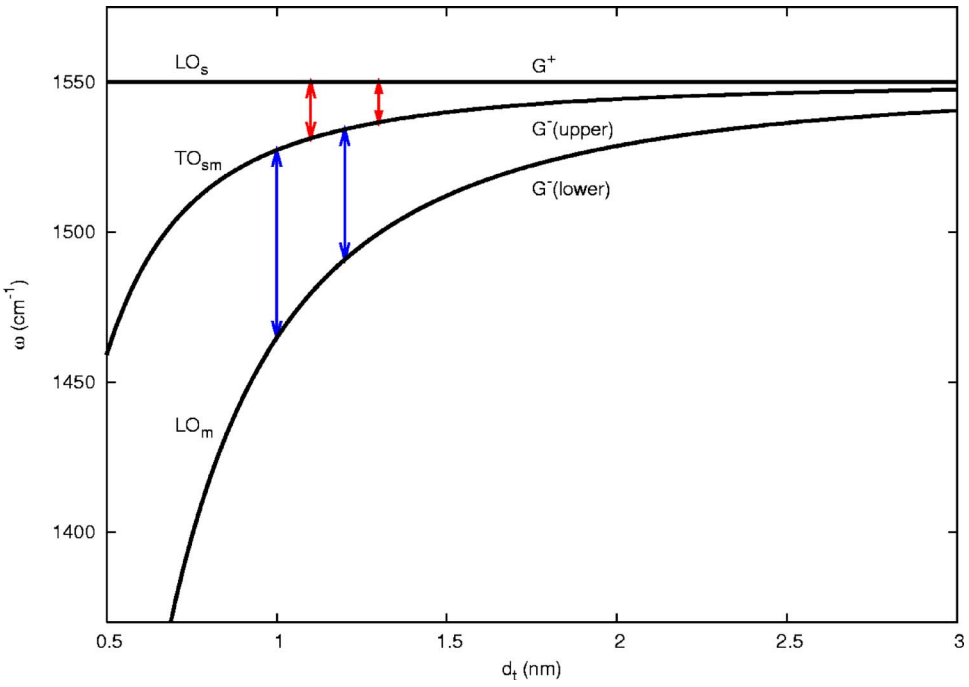

FIG. 6. (Color online) Sketch of the G-band dispersion law with nanotube diameter at $\mathbf{\Gamma}_0$. The vertical arrows connect branches related to LO-TO splitting.

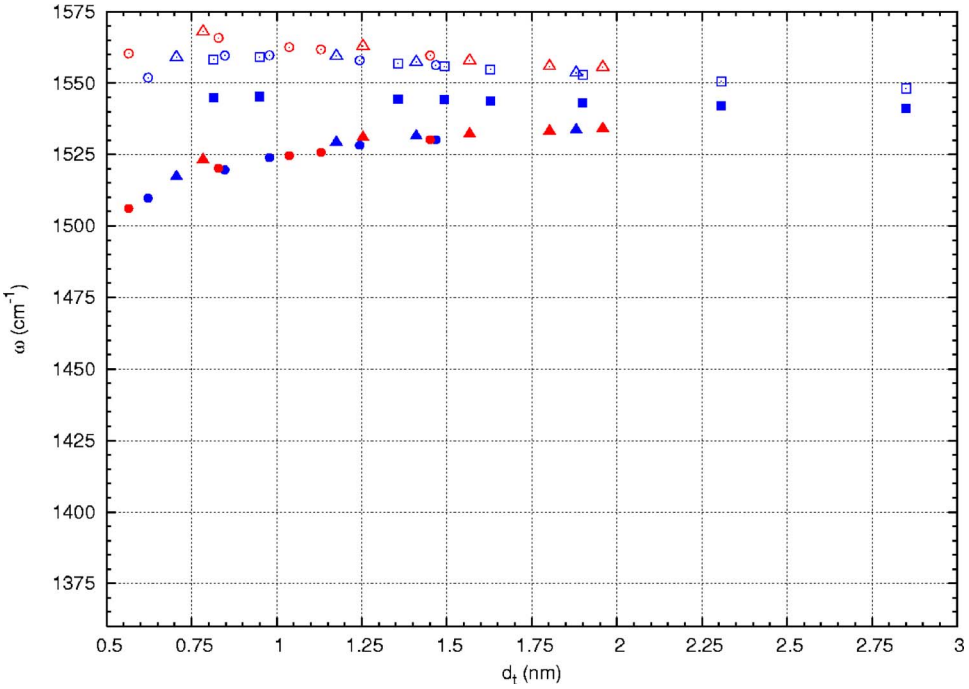

FIG. 7. (Color online) Phonons at Γ_1 (i.e., $\mu=1$, $\xi=0$): diameter dependence of the G^+ and G^- peaks in the Raman spectra of nanotubes. Red symbols are for semiconducting nanotubes, blue symbols for metallic tubes. Solid symbols are for LO modes; open symbols are for TO modes. Triangles denote zigzag nanotubes; squares denote armchair and circles chiral nanotubes.

G^- LO band for metallic nanotubes is expected to show a strong Kohn anomaly and a large electron-phonon coupling.[6] In agreement with this finding we have LO modes which are strongly diameter dependent (see Fig. 5). On the contrary, the TO modes are fairly sensitive to the diameter and are not affected by the Kohn anomaly. Thus, as far as the Γ_0 TO phonons are concerned, all the nanotubes contribute with the same dispersion law to the G^- upper branch (the central branch of Figs. 5 and 6). On the other hand, the LO modes are very sensitive to the EPC; therefore, two distinct branches are found for metallic and semiconducting nanotubes:

(a) the G^+ branch to which semiconducting nanotubes contribute and

(b) the G^- lower branch due to metallic nanotubes (strong EPC).

Finally, it is important to point out that armchair and zigzag nanotubes have, respectively, LO and TO modes at Γ_0 which are symmetry forbidden in the Raman spectra (they are of ungerade symmetry species). This result agrees with a recent work.[21] In Fig. 5 the black symbols indicate frequencies of these symmetry-forbidden phonons.

The assignment so obtained partially agrees and partially disagrees with previous works.[1,6,22,23]

(a) According to Ref. 1 the G^+ is due to longitudinal modes of both semiconducting and metallic nanotubes; for us, it is due to longitudinal modes of just the semiconducting nanotubes.

(b) According to Ref. 1 the G^- upper branch corresponds to transversal modes of semiconducting nanotubes; for us, it corresponds to the transversal mode of both metallic and semiconducting nanotubes.

(c) According to Ref. 1 the G^- lower branch is due to the transversal modes of metallic nanotubes; for us, it is due to the longitudinal mode of metallic nanotubes.

(d) According to Ref. 6 the transversal mode of metallic nanotubes does not disperse because the model adopted in Ref. 6 does not account for curvature effects; for us, it shows a modest dispersion and it is associated with the G^- upper branch (TO_{sm}).

(e) According to Ref. 6 the G^- lower branch is the longitudinal mode of metallic nanotubes and we agree on this point. Note that Ref. 6 does not present any calculation for semiconducting nanotubes.

According to point (a) of the above analysis we find only frequencies of semiconducting nanotubes in the G^+ branch, contrary to experiments[1] which show in the G^+ branch also contributions from metallic nanotubes. A possible explanation is that the phonons of metallic nanotubes experimentally observed on the G^+ branch are not Γ_0 phonons. In particular, inspection of the phonons at Γ_1 point (see Fig. 7) clearly shows the presence of metallic nanotubes on a nondispersive branch which can be put in correspondence with the G^+ experimental data. This observation allows us to overcome the apparent disagreement of our results for the Γ_0 phonons.

Let us now consider the G^- upper branch. At Γ_0 we have phonons of both metallic and semiconducting nanotubes on this branch. According to experiments[1] the G^- upper branch is mainly composed of phonons belonging to semiconducting nanotubes and just a minority of phonons of metallic nanotubes is found here. This suggests that the intensity of TO modes of metallic nanotubes is weak for phonons at Γ_0. We summarize in Fig. 8 the dispersion of the G modes at Γ_0 and Γ_1 to ease the overall understanding of the data.

We may ask also if the other Raman-active vibrational frequencies in our model do depend so strongly on the electronic structure as the G band. It is known that the RBM frequency shows a linear dispersion with the nanotube diameter, independently of the metallic and semiconducting nature of the nanotube.[24] In Fig. 9(a) we report the square roots of the eigenvalues of the $\mathbf{G}$ matrix ($\sqrt{\lambda_G}$) relative to radial vibrational displacements of the nanotubes of Table I. These eigenvalues can be related to the frequencies of a hypotheti-

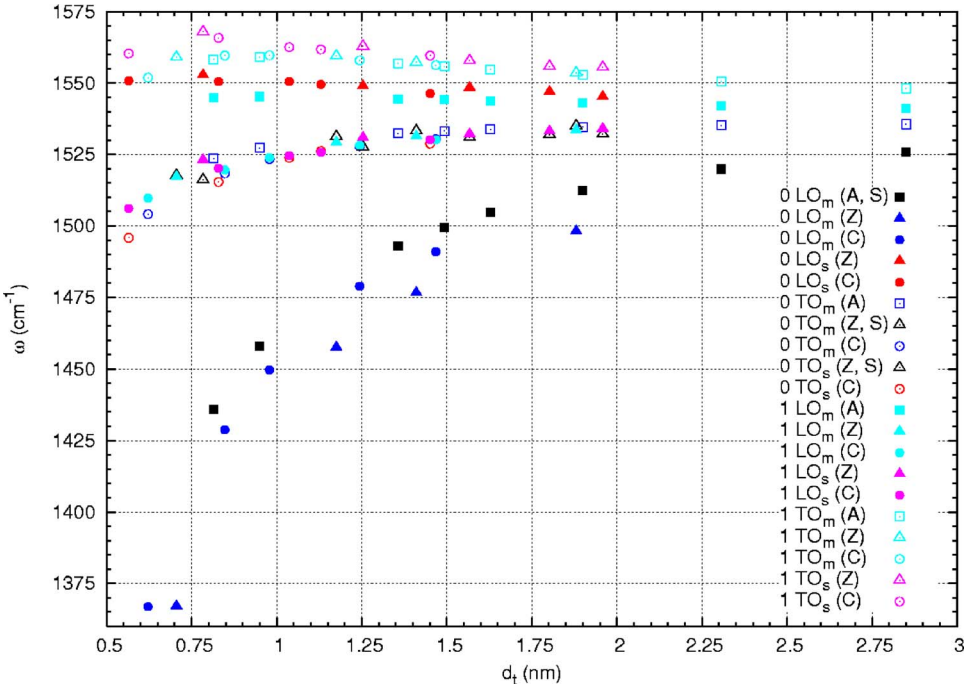

FIG. 8. (Color online) Diameter dependence of the G^+ and G^- peaks in the Raman spectra of nanotubes ($\mathbf{\Gamma}_0$ and $\mathbf{\Gamma}_1$ phonons). Labels for phonons at $\mathbf{\Gamma}_0$: red symbols semiconducting nanotubes, blue symbols metallic nanotubes. Labels for phonons at $\mathbf{\Gamma}_1$: magenta symbols, semiconducting nanotubes; cyan symbols, metallic nanotubes; solid symbols indicate LO mode, and open symbols indicate TO modes. Triangles denote zigzag (Z) nanotubes; squares denote armchair (A) and circles chiral (C) nanotubes. Black symbols indicate silent (S) modes in the Raman spectra of achiral nanotubes.

cal dynamical problem where the force field is the identity matrix. In this way only the effect of kinetic coupling is taken into account. It is evident that even without the inclusion of the true force constant matrix **F** in the dynamical problem [Eq. (1)] we anyway recover the right linear dispersion versus the inverse diameter.[24] In Fig. 9(b) the same dispersion is showed for the square roots of the eigenvalues of the complete dynamical problem [Eq. (1)]. Since for both Figs. 9(a) and 9(b) a similar linear dispersion is obtained, one can conclude that the force field (which is different for each nanotube) does not influence the linear dispersion of the RBM frequencies versus the inverse diameter. Therefore the observed linear change of the RBM frequency with respect to the inverse diameter is due to a purely kinetic effect (i.e., it is related to the curvature of the nanotube and to the **G** matrix alone). This allows to define for the case of the RBM a universal effective force constant $k_{eff}=4.57\ N/\mathrm{cm}$ for any nanotube ($\omega_{RBM}=\sqrt{k_{\mathrm{eff}}\lambda_G}$).

IV. CONCLUSIONS

We have introduced a general model which allows to describe the vibrational dynamics of any (n,m) nanotube while keeping reduced to a minimum the number of degrees of freedom (three stretchings + six bendings). The proposed valence force field can cope with the different electronic structures of metallic and semiconducting nanotubes and gives the expected Kohn anomaly behaviour[6] for metallic nanotubes. In particular, this is due to the correct decay with distance of the off-diagonal CC stretching force constants in real space. Within this frame we propose an assignment of the G band in the Raman spectra of SWNT's. In particular, considering phonons at $\mathbf{\Gamma}_0$, we assign the G^- lower branch to LO modes of metallic nanotubes and the G^+ branch to LO modes of semiconducting nanotubes. The G^- upper branch is assigned to TO modes of semiconducting and metallic nanotubes at $\mathbf{\Gamma}_0$. A computation of Raman cross sections is needed to fully understand the reason why only a few metallic nanotubes are experimentally found to contribute to the G^- upper branch. Moreover, it is necessary to consider also phonons at $\mathbf{\Gamma}_1$ in order to account for the experimentally observed[1] contributions to the G^+ branch arising from metallic nanotubes. It is also important to point out that the LO modes of armchair nanotubes at $\mathbf{\Gamma}_0$ and the TO modes of zigzag nanotubes at $\mathbf{\Gamma}_0$ are ungerade and thus are symmetry forbidden in the Raman spectrum. Finally our valence force field correctly accounts for the right dispersion of the RBM with respect to the inverse diameter.

ACKNOWLEDGMENT

This work was supported by a grant from the Italian Ministry of Education, University and Research (FIRB project "Carbon based micro and nano structures," RBNE019NKS).

APPENDIX A: THE CHIRAL GEOMETRY OF NANOTUBES

The coordinates $\mathbf{X}_{n_1,n_2}$ of the carbon atoms belonging to the (n_1,n_2) cell of a generic (n,m) nanotube can be obtained by rototranslation of the coordinates $\mathbf{X}_{0,0}$ of the (0,0) reference cell. The coordinates $\mathbf{X}_{0,0}$ can be easily obtained by taking the coordinates of the two carbons of the fundamental cell of graphene and "wrapping" them around the cylinder of radius $R=|\mathbf{C}_h|/2\pi$ (see Fig. 10). The trasformation mapping the coordinates of the reference cell of the nanotube into the coordinates of the generic (n_1,n_2) cell is

$$\mathbf{X}_{n_1,n_2}=\mathbf{W}(n_1\phi_1+n_2\phi_2)\mathbf{X}_{0,0}+(n_1\tau_1+n_2\tau_2)\mathbf{T}, \quad \text{(A1)}$$

where $\mathbf{W}(\alpha)$ stands for the rotation of the angle α around the Y axis (axis of the nanotube) and $\mathbf{T}$ is the fundamental trans-

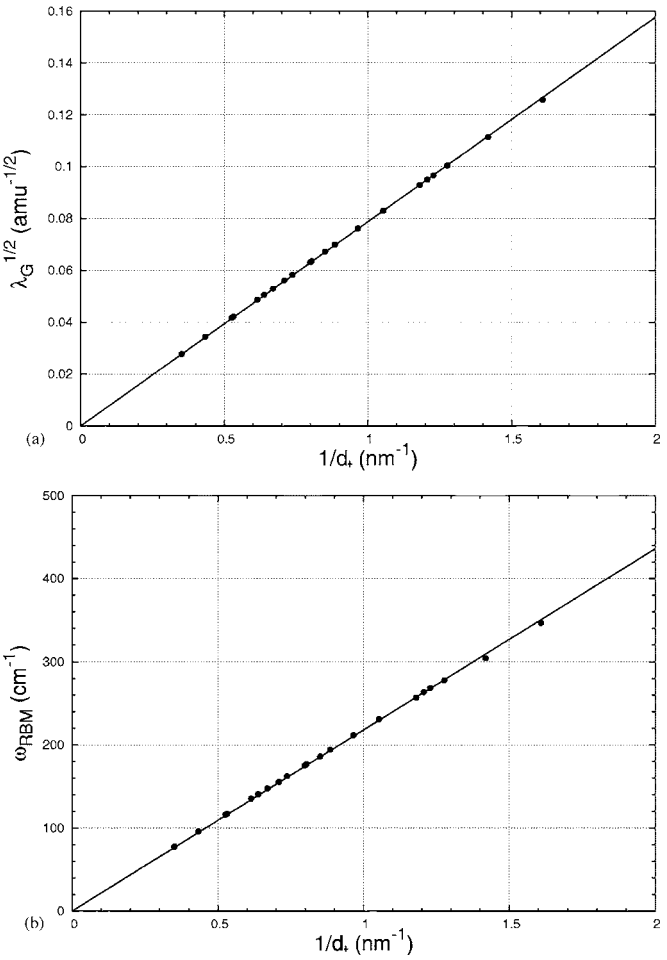

FIG. 9. Linear dispersion of the RBM mode versus the inverse diameter of the nanotube: (a) square roots of the eigenvalues of the **G** matrix and (b) RBM frequencies predicted solving the full dynamical problem, Eq. (1).

lation vector of the nanotube (see Fig. 10). The parameters $\phi_{1,2}$ and $\tau_{1,2}$ in Eq. (A1) are related to the projections of the fundamental vectors of graphene $\mathbf{a}_1$ and $\mathbf{a}_2$ along the fundamental vectors $\mathbf{C}_h$ and $\mathbf{T}$ of the nanotube. In particular,

$$\phi_1 = 2\pi \frac{\mathbf{a}_1 \cdot \mathbf{C}_h}{|\mathbf{C}_h|^2},$$

$$\phi_2 = 2\pi \frac{\mathbf{a}_2 \cdot \mathbf{C}_h}{|\mathbf{C}_h|^2},$$

$$\tau_1 = \frac{\mathbf{a}_1 \cdot \mathbf{T}}{|\mathbf{T}|^2},$$

$$\tau_2 = \frac{\mathbf{a}_2 \cdot \mathbf{T}}{|\mathbf{T}|^2}, \tag{A2}$$

where the vectors $\mathbf{C}_h$ and $\mathbf{T}$ are given by

$$\mathbf{C}_h = n\mathbf{a}_1 + m\mathbf{a}_2,$$

$$\mathbf{T} = t_1\mathbf{a}_1 + t_2\mathbf{a}_2, \tag{A3}$$

and t_1 and t_2 are[25]

$$t_1 = \frac{2m+n}{d_R},$$

$$t_2 = -\frac{2n+m}{d_R},$$

$$d_R = gcd(2n+m, 2m+n). \tag{A4}$$

In our calculations the carbon-carbon bond length a_{CC} has been fixed at the value of 1.421 Å. By expanding the scalar products in Eqs. (A2), we obtain

$$\phi_1 = 2\pi \frac{2n+m}{2(n^2+nm+m^2)},$$

$$\phi_2 = 2\pi \frac{2m+n}{2(n^2+nm+m^2)},$$

$$\tau_1 = \frac{md_R}{2(n^2+nm+m^2)},$$

$$\tau_2 = -\frac{nd_R}{2(n^2+nm+m^2)}. \tag{A5}$$

These parameters allow us to generate the Cartesian coordinates of the carbon atoms of the nanotube in three dimensions according to Eq. (A1). In particular, the rotation matrix **W** of Eq. (A1) is given by

$$\mathbf{W}(\phi) = \begin{pmatrix} \cos\phi & 0 & -\sin\phi \\ 0 & 1 & 0 \\ \sin\phi & 0 & \cos\phi \end{pmatrix}. \tag{A6}$$

The coordinates $\mathbf{X}_{0,0}$ of the two carbon atoms in the rototranslational minimal cell of the nanotube are obtained by trasforming the coordinates of the **P** point lying on the graphene plane (x,y) into the coordinates of the point $\mathbf{P}'$ lying on the surface of the cylinder of radius $R=|\mathbf{C}_h|/2\pi$ (see Fig. 10). This is accomplished by means of the following equation:

$$(\mathbf{P}' - \mathbf{O}) = (\mathbf{K} - \mathbf{O}) + \rho\mathbf{v}_t + R(\cos\Phi\boldsymbol{\xi} + \sin\Phi\boldsymbol{\eta}), \tag{A7}$$

where Φ and ρ are given by

$$\Phi = 2\pi \frac{(\mathbf{P}-\mathbf{O})\cdot\boldsymbol{\eta}}{|\mathbf{C}_h|}, \tag{A8}$$

$$\rho = (\mathbf{P}-\mathbf{O})\cdot\mathbf{v}_t. \tag{A9}$$

See Fig. 10 for the definition of the unit vectors $\boldsymbol{\xi}$, $\boldsymbol{\eta}$, and $\mathbf{v}_t$.

This procedure allows us to trasform the planar coordinates of the carbons on the graphene plane (x,y) (see Fig. 1) into the fully three-dimensional coordinates needed to calcu-

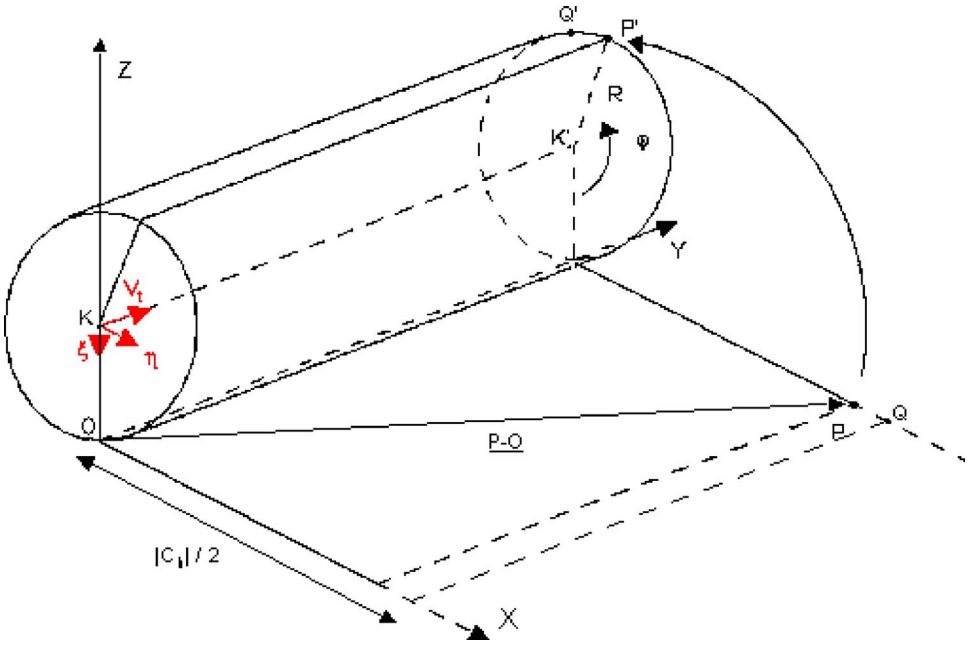

FIG. 10. (Color online) The cylinder of radius $R=|\mathbf{C}_h|/2\pi$ used to construct the fully three-dimensional geometry of the generic (n,m) nanotube starting from the graphene plane.

late the $\mathbf{s}_i^R$ Wilson vectors which enter the definition of the **B** matrix of Eq. (3). Before applying the trasformation (A1) to generate the coordinates of the atoms of the whole nanotube in the (X,Y,Z) Cartesian system shown in Fig. 10, it is necessary to introduce a translation which brings the origin in the **K** point of Fig. 10 and a rotation around the $z \equiv Z$ axis which aligns the X and Y axes along the vectors $\mathbf{C}_h$ and **T**, respectively:

$$\mathbf{W}'\left(\chi-\frac{\pi}{6}\right)=\begin{pmatrix}\cos\left(\chi-\frac{\pi}{6}\right) & -\sin\left(\chi-\frac{\pi}{6}\right) & 0\\ \sin\left(\chi-\frac{\pi}{6}\right) & \cos\left(\chi-\frac{\pi}{6}\right) & 0\\ 0 & 0 & 1\end{pmatrix} \tag{A10}$$

(χ is the chiral angle which is called θ elsewhere[25]).

The $\mathbf{B}(\theta_1,\theta_2)$ matrix transforms the Cartesian coordinates into internal coordinates; therefore, in our case it is a 9×6 matrix. The five **B** matrices showing up on the right-hand side of Eq. (3) are defined as follows:

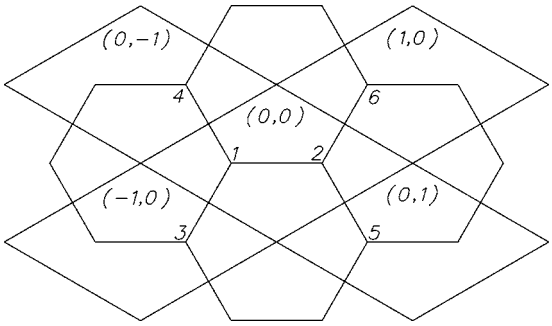

FIG. 11. Atom numbering for carbons in cell (0,0) and nearest neighbors.

$$\left[\begin{array}{cc|cc|cc|cc|cc}
\mathbf{B}_{00} & & \mathbf{B}_{10} & & \mathbf{B}_{\bar{1}0} & & \mathbf{B}_{01} & & \mathbf{B}_{0\bar{1}} & \\
\hline
\mathbf{s}_1^{R_1} & \mathbf{s}_2^{R_1} & \mathbf{0} & \mathbf{0} & \mathbf{0} & \mathbf{0} & \mathbf{0} & \mathbf{0} & \mathbf{0} & \mathbf{0} \\
\mathbf{s}_1^{R_2} & \mathbf{0} & \mathbf{0} & \mathbf{0} & \mathbf{0} & \mathbf{s}_3^{R_2} & \mathbf{0} & \mathbf{0} & \mathbf{0} & \mathbf{0} \\
\mathbf{s}_1^{R_3} & \mathbf{0} & \mathbf{0} & \mathbf{0} & \mathbf{0} & \mathbf{0} & \mathbf{0} & \mathbf{0} & \mathbf{0} & \mathbf{s}_4^{R_3} \\
\hline
\mathbf{s}_1^{\omega_1} & \mathbf{0} & \mathbf{0} & \mathbf{0} & \mathbf{0} & \mathbf{s}_3^{\omega_1} & \mathbf{0} & \mathbf{0} & \mathbf{0} & \mathbf{s}_4^{\omega_1} \\
\mathbf{s}_1^{\omega_2} & \mathbf{s}_2^{\omega_2} & \mathbf{0} & \mathbf{0} & \mathbf{0} & \mathbf{0} & \mathbf{0} & \mathbf{0} & \mathbf{0} & \mathbf{s}_4^{\omega_2} \\
\mathbf{s}_1^{\omega_3} & \mathbf{s}_2^{\omega_3} & \mathbf{0} & \mathbf{0} & \mathbf{0} & \mathbf{s}_3^{\omega_3} & \mathbf{0} & \mathbf{0} & \mathbf{0} & \mathbf{0} \\
\mathbf{0} & \mathbf{s}_2^{\omega_1'} & \mathbf{s}_6^{\omega_2'} & \mathbf{0} & \mathbf{0} & \mathbf{0} & \mathbf{s}_5^{\omega_1'} & \mathbf{0} & \mathbf{0} & \mathbf{0} \\
\mathbf{s}_1^{\omega_2'} & \mathbf{s}_2^{\omega_2'} & \mathbf{0} & \mathbf{0} & \mathbf{0} & \mathbf{0} & \mathbf{s}_5^{\omega_2'} & \mathbf{0} & \mathbf{0} & \mathbf{0} \\
\mathbf{s}_1^{\omega_3'} & \mathbf{s}_2^{\omega_3'} & \mathbf{s}_6^{\omega_3'} & \mathbf{0} & \mathbf{0} & \mathbf{0} & \mathbf{0} & \mathbf{0} & \mathbf{0} & \mathbf{0}
\end{array}\right]. \tag{A11}$$

The vectors $\mathbf{s}_i^R$ are the so-called Wilson's vectors[5] relative to the ith atom and defining the Rth internal coordinate (see Figs. 1 and 11). The Wilson's vectors are known functions of the Cartesian coordinates of the atoms involved in the definition of the internal coordinate considered.[5]

APPENDIX B: ELECTRONIC STRUCTURE OF NANOTUBES WITHIN HÜCKEL THEORY

The so-called zone-folding procedure[24] introduced for describing the peculiar periodic boundary conditions of nanotubes can be easily derived by starting from the consideration that the generic wave vector $\mathbf{k}=(2\pi)^{-1}(\theta_1\mathbf{b}_1+\theta_2\mathbf{b}_2)$ must satisfy the conditions given by Eqs. (5). By expanding the scalar products of Eqs. (5) while keeping in mind the definition of $\mathbf{C}_h$ and **T** [Eq. (A3)] one finds

$$n\theta_1 + m\theta_2 = 2\pi\mu,$$

$$t_1\theta_1 + t_2\theta_2 = \xi. \tag{B1}$$

These coupled equations can be cast in the more convenient form wich expresses θ_1 and θ_2 as a function of the nanotube quantum numbers ξ and μ. By solving Eqs. (B1) in terms of θ_1 and θ_2 and by making use of relationships (A4) one gets

$$\theta_1 = \frac{2\pi(2n+m)\mu}{2(n^2+nm+m^2)} + \frac{md_R\xi}{2(n^2+nm+m^2)},$$

$$\theta_2 = \frac{2\pi(2m+n)}{2(n^2+nm+m^2)} - \frac{nd_R\xi}{2(n^2+nm+m^2)}. \tag{B2}$$

By employing in Eqs. (B2) the relations given by Eqs. (A5) one finally obtains Eqs. (4).

APPENDIX C: BOND ORDERS AND BOND-BOND POLARIZABILITY INTEGRALS

The calculation of the quantities p_i and Π_{ij} defined in Eq. (11) is needed for the determination of the force field constants f_{ij} [see Eqs. (8)]. This requires the evaluation of the integrand functions q_i and π_{ij} which can be obtained directly from the knowledge of the LCAO coefficients C of the nanotube crystal orbitals and the orbital energies ε. These can be expressed conveniently as follows (the orbital energies are given in units of the hopping integral β_0, as customary in Hückel theory):

$$\mathbf{C}_o = \frac{1}{\sqrt{2}}\begin{pmatrix} e^{i\eta/2} \\ e^{-i\eta/2} \end{pmatrix},$$

$$\mathbf{C}_e = \frac{1}{\sqrt{2}}\begin{pmatrix} e^{i\eta/2} \\ -e^{-i\eta/2} \end{pmatrix},$$

$$\varepsilon_o = -|f(\boldsymbol{\theta})|, \quad \varepsilon_e = |f(\boldsymbol{\theta})|. \tag{C1}$$

The orbital energies ε and the quantity $\eta = \arg f$ are given through the function $f(\boldsymbol{\theta})$ which is defined as

$$f(\theta_1,\theta_2) = 1 + e^{i\theta_1} + e^{i\theta_2}. \tag{C2}$$

This form of the LCAO coefficients is the same obtained in a Hückel theory treatment of graphite (see, for instance, Ref. 4). The important difference here is that not all the **k** points within the first Brillouin zone of graphene are allowed, but just those satisfying the boundary conditions specific to nanotubes. This fact restricts the allowed values of the phases θ_1 and θ_2 (and θ_1' and θ_2') to those given by Eq. (4). By combining the LCAO coefficients and orbital energies given by Eqs. (C1) with the general expressions for the bond orders and BBP's [Eqs. (10)] one can derive the explicit expressions for the quantities appearing in Eqs. (11). In particular, the integrand functions q_i which allow one to compute the bond orders of the three nonequivalent CC bonds in the cell are given by

$$q_1 = \cos\,\eta,$$

$$q_2 = \cos(\eta - \theta_1),$$

$$q_3 = \cos(\eta - \theta_2). \tag{C3}$$

By introducing a suitable common prefactor g [similarly to $\boldsymbol{\theta}$ defined above, $\mathbf{n}$ represents the vector (n_1,n_2)],

$$g_{\mathbf{n}}(\boldsymbol{\theta},\boldsymbol{\theta}') = -\frac{1}{4}\frac{e^{i\mathbf{n}\cdot(\boldsymbol{\theta}-\boldsymbol{\theta}')}}{|f(\boldsymbol{\theta})| + |f(\boldsymbol{\theta}')|}, \tag{C4}$$

the integrand functions $\pi_{i_{(0,0)}j_{(n_1,n_2)}}$ needed to compute all the necessary BBP's are given by

$$\pi_{11} = g_{\mathbf{n}}(\boldsymbol{\theta},\boldsymbol{\theta}')[2 - e^{i(\eta+\eta')} - e^{-i(\eta+\eta')}] + \text{c.c.},$$

$$\pi_{22} = g_{\mathbf{n}}(\boldsymbol{\theta},\boldsymbol{\theta}')[2 - e^{i(\eta+\eta'-\theta_1-\theta_1')} - e^{-i(\eta+\eta'-\theta_1-\theta_1')}] + \text{c.c.},$$

$$\pi_{33} = g_{\mathbf{n}}(\boldsymbol{\theta},\boldsymbol{\theta}')[2 - e^{i(\eta+\eta'-\theta_2-\theta_2')} - e^{-i(\eta+\eta'-\theta_2-\theta_2')}] + \text{c.c.},$$

$$\pi_{12} = g_{\mathbf{n}}(\boldsymbol{\theta},\boldsymbol{\theta}')[e^{i\theta_1'}(1 - e^{-i(\eta+\eta')}) + e^{-i\theta_1}(1 - e^{i(\eta+\eta')})] + \text{c.c.},$$

$$\pi_{13} = g_{\mathbf{n}}(\boldsymbol{\theta},\boldsymbol{\theta}')[e^{i\theta_2'}(1 - e^{-i(\eta+\eta')}) + e^{-i\theta_2}(1 - e^{i(\eta+\eta')})] + \text{c.c.},$$

$$\pi_{23} = g_{\mathbf{n}}(\boldsymbol{\theta},\boldsymbol{\theta}')[e^{i(\theta_2'-\theta_1')} - e^{i(\eta+\eta'-\theta_1'-\theta_2)} - e^{-i(\eta+\eta'-\theta_2'-\theta_1)} + e^{i(\theta_1-\theta_2)}] + \text{c.c.} \tag{C5}$$

The different behavior of metallic versus semiconducting nanotubes (see Fig. 2) is related to the inclusion of the **K** and **K′** points (at the corner of the first Brillouin zone of graphene) in the integration domain for metallic nanotubes [see discussion relative to Eq. (11)]. In fact, the function $f(\theta_1,\theta_2)$ equals zero when it is evaluated in correspondence with the **K** or **K′** points. For metallic nanotubes this results in a slower decrease of the function $g_{\mathbf{n}}(\boldsymbol{\theta},\boldsymbol{\theta}')$ while increasing the intercell indexes **n**. This directly affects the BBP Π_{ij} and causes the slower decay shown in Fig. 2.

[1] A. Jorio, A. G. Souza Filho, G. Dresselhaus, M. S. Dresselhaus, A. K. Swan, M. S. Ünlü, B. B. Goldberg, M. A. Pimenta, J. H. Hafner, C. M. Lieber, and R. Saito, Phys. Rev. B **65**, 155412 (2002).

[2] L. Piseri, R. Tubino, and G. Dellepiane, Solid State Commun. **44**, 1589 (1982).

[3] L. Piseri, R. Tubino, L. Paltrinieri, and G. Dellepiane, Solid State Commun. **46**, 183 (1983).

[4] C. Mapelli, C. Castiglioni, G. Zerbi, and K. Müllen, Phys. Rev. B **60**, 12710 (1999).

[5] E. B. Wilson, J. C. Decius, and P. C. Cross, *Molecular Vibrations: The theory of infrared and Raman vibrational spectra*

(McGraw-Hill, New York, 1955).
[6] M. Lazzeri, S. Piscanec, F. Mauri, A. C. Ferrari, and J. Robertson, Phys. Rev. B **73**, 155426 (2006).
[7] S. Piscanec, M. Lazzeri, F. Mauri, A. C. Ferrari, and J. Robertson, Phys. Rev. Lett. **93**, 185503 (2004).
[8] C. A. Coulson and H. C. Longuet-Higgins, Proc. R. Soc. London, Ser. A **191**, 39 (1947).
[9] C. A. Coulson and H. C. Longuet-Higgins, Proc. R. Soc. London, Ser. A **192**, 16 (1947).
[10] C. A. Coulson and H. C. Longuet-Higgins, Proc. R. Soc. London, Ser. A **193**, 447 (1947).
[11] T. Kakitani, Prog. Theor. Phys. **51**, 656 (1974).
[12] K. Ohno, J. Chem. Phys. **95**, 5524 (1995).
[13] C. Castiglioni, F. Negri, M. Tommasini, E. Di Donato, and G. Zerbi, in *Carbon—The Future Material for Advanced Tecnology Applications*, edited by G. Messina and S. Santangelo (Springer, Heidelberg, 2006).
[14] S. Califano, *Vibrational States* (Wiley, New York, 1976); S. Califano and B. Crawford, Z. Elektrochem. **64**, 571 (1960).
[15] L. Piseri and G. Zerbi, J. Mol. Spectrosc. **26**, 254 (1968); J. Chem. Phys. **48**, 3561 (1968).
[16] W. Rhodes, J. Chem. Phys. **37**, 2433 (1962).
[17] $N=A_t/A_g$ where A_t is the area of translational cell $(\mathbf{T},\mathbf{C}_h)$ of the nanotube and A_g is the area of the graphene unit cell.
[18] Carter T. White and John W. Mintmire, J. Phys. Chem. B **109**, 52 (2005).
[19] Note that the higher frequency modes at $\mathbf{\Gamma}_0$ correspond to the G mode of graphite of the E_{2g} species.
[20] The bond orders are dimensionless quantities, while the BBP's have units of inverse energy. We adopt here the usual convention of expressing energies in units of the hopping integral (at equilibrium bond length) β_0.
[21] J. Jiang, R. Saito, A. Grüneis, S. G. Chou, Ge. G. Samsonidze, A. Jorio, G. Dresselhaus, and M. S. Dresselhaus, Phys. Rev. B **71**, 205420 (2005).
[22] S. D. M. Brown, A. Jorio, P. Corio, M. S. Dresselhaus, G. Dresselhaus, R. Saito, and K. Kneipp, Phys. Rev. B **63**, 155414 (2001).
[23] M. Oron-Carl, F. Hennrich, M. M. Kappes, H. von Löhneysen, and R. Krupke, Nano Lett. **5**, 1761 (2005).
[24] M. S. Dresselhaus and P. C. Eklund, Adv. Phys. **49**, 705 (2000).
[25] *Carbon Nanotubes—Synthesis, Structure, Properties and Applications*, edited by M. S. Dresselhaus, G. Dresselhaus, and Ph. Avouris (Springer, Berlin, 2001).